# Modeling of the Influence of Sea Ice Cycle and Langmuir Circulation on the Upper Ocean Mixed Layer Depth and Freshwater Distribution at the West Antarctic Peninsula

Cristina Schultz[1], Scott C. Doney[1], Weifeng Gordon Zhang[2], Heather C Regan[3], Paul Holland[4], Michael Meredith[4], and Sharon Stammerjohn[5]

[1]University of Virginia
[2]Woods Hole Oceanographic Institution
[3]Laboratoire d'Océanographie Physique et Spatiale
[4]British Antarctic Survey
[5]U. of Colorado, Boulder

November 26, 2022

**Abstract**

The Southern Ocean is chronically under-sampled due to its remoteness, harsh environment and sea-ice cover. Ocean circulation models yield significant insight into key processes and to some extent obviate the dearth of data, however they often underestimate surface mixed layer depth (MLD), with consequences for water-column properties. In this study, a coupled circulation and sea-ice model was implemented for the region adjacent to the West Antarctic Peninsula (WAP), a climatically sensitive region which has exhibited decadal trends toward higher temperatures, a shorter sea-ice season and increasing glacial freshwater input, overlain by strong interannual variability. Hindcast simulations were conducted with different air-ice drag coefficients and Langmuir-circulation parameterizations to determine the impact of these factors on MLD. Including Langmuir circulation deepened the surface mixed layer, with the deepening being more pronounced in the shelf and slope regions. Optimal selection of an air-ice drag coefficient also increased the modeled MLD by similar amounts, and had a larger impact in improving the reliability of the simulated MLD interannual variability. This study highlights the importance of sea ice volume and redistribution to correctly reproduce the physics of the underlying ocean, and the potential of appropriately parameterizing Langmuir circulation to help correct for a bias towards shallow MLD in the Southern Ocean. The model also reproduces observed freshwater patterns in the WAP during late summer and suggests that areas of intense summertime sea-ice melt can still show net annual freezing due to high sea-ice formation during the winter.

# Modeling of the Influence of Sea Ice Cycle and Langmuir Circulation on the Upper Ocean Mixed Layer Depth and Freshwater Distribution at the West Antarctic Peninsula

**C. Schultz[1], S. C. Doney[1], W. G. Zhang[2], H. Regan[3], P. Holland[4], M. Meredith[4], S. Stammerjohn[5]**

[1] University of Virginia, Department of Environmental Sciences, Charlottesville, VA, USA
[2] Woods Hole Oceanographic Institution, Woods Hole, MA, USA
[3] Univ. Brest, CNRS, IRD, Ifremer, Laboratoire D'Océanographie Physique et Spatiale, IUEM, Brest, France
[4] British Antarctic Survey, Natural Environment Research Council, Cambridge, UK
[5] Institute of Arctic and Alpine Research, University of Colorado, Boulder, CO, USA

Corresponding author: Cristina Schultz (cs3xm@virginia.edu)

- Sea-ice redistribution had a large impact on the mixed layer depth seasonality and interannual variability in the West Antarctic Peninsula
- In the West Antarctic Peninsula, areas of high summer sea-ice melt can show net annual freezing due to high sea-ice formation in winter
- Including a parameterization for Langmuir Circulation based on entrainment below the mixed layer improved the simulated mixed layer depth

**Abstract**

The Southern Ocean is chronically under-sampled due to its remoteness, harsh environment and sea-ice cover. Ocean circulation models yield significant insight into key processes and to some extent obviate the dearth of data, however they often underestimate surface mixed layer depth (MLD), with consequences for water-column properties. In this study, a coupled circulation and sea-ice model was implemented for the region adjacent to the West Antarctic Peninsula (WAP), a climatically sensitive region which has exhibited decadal trends toward higher temperatures, a shorter sea-ice season and increasing glacial freshwater input, overlain by strong interannual variability. Hindcast simulations were conducted with different air-ice drag coefficients and Langmuir-circulation parameterizations to determine the impact of these factors on MLD. Including Langmuir circulation deepened the surface mixed layer, with the deepening being more pronounced in the shelf and slope regions. Optimal selection of an air-ice drag coefficient also increased the modeled MLD by similar amounts, and had a larger impact in improving the reliability of the simulated MLD interannual variability. This study highlights the importance of sea ice volume and redistribution to correctly reproduce the physics of the underlying ocean, and the potential of appropriately parameterizing Langmuir circulation to help correct for a bias towards shallow MLD in the Southern Ocean. The model also reproduces observed freshwater patterns in the WAP during late summer and suggests that areas of intense summertime sea-ice melt can still show net annual freezing due to high sea-ice formation during the winter.

## 1 Introduction

The coastal ocean on the western side of the West Antarctic Peninsula (WAP) has undergone dramatic changes over the past several decades. During the second half of the 20$^{th}$ century, the WAP region showed the highest atmospheric warming in the Southern Hemisphere (Vaughan et al, 2003), a decrease in the duration of the sea-ice season (Stammerjohn et al., 2008) and an accelerating retreat of 80 % of the glaciers in the region (Cook et al, 2005). The surface ocean also exhibited an increase in temperature of more than 1˚C (Meredith et al., 2005). The increased surface ocean temperature, thought to be caused by increased temperatures in the atmosphere and the decreased sea-ice cover, could lead to positive feedbacks that would further increase the atmospheric warming. Around the turn of the 21$^{st}$ century, however, the atmospheric warming trend leveled off and even reversed direction in some places (Turner et al., 2016). This trend reversal can be attributed to natural climate variability and indicates that the changes observed in the WAP cannot be explained by large-scale global warming alone.

The impact of changes in heat and freshwater input on the vertical ocean mixing have not been fully quantified. While sea-ice melt decreases density of the surface layer and contributes to stronger near-surface stratification, decreased sea-ice cover also leads to increased wind-induced ocean mixing. The effect of sea-ice changes on the surface mixed layer depth (MLD), therefore, relies on a balance between these two competing effects, which is further complicated by laterally redistributing and mechanically thickening sea ice cover. This can also redistribute sea ice melt waters away from where sea ice was formed in situ, thus leading to areas of net sea ice production versus sea ice melt (Meredith et.al., 2008; 2010; 2017).

Studying the impact of each of these changes on the MLD is important given it may affect not only trends in the distribution of water masses in the region, but also on oceanic primary production, ecosystem dynamics and carbon cycle in the WAP (Vernet et. al., 2008; Legge et. al., 2017). Understanding the impact of increased glacial melt is also important given salinity gradients are thought to contribute to the coastal circulation in the WAP (Moffat et al., 2008), and glacial freshwater can be a major source of dissolved iron for primary production (Annett et al., 2017).

One of the challenges of studying the MLD in the WAP is the scarcity of data. Although the Palmer- Long Term Ecological Research (LTER) project has been conducting yearly cruises during January and February since 1993, thus providing an invaluable dataset of over two decades of duration, each cruise constitutes a snapshot relevant to the period of its occupation (Ducklow et al., 2013). Sustained time series with high-frequency sampling exist, including the Rothera Time Series (REF) and stations occupied quasi-weekly adjacent to Palmer Station (Figure 1), however these point measurements at near-coastal sites do not have full spatial extent across the WAP shelf.

Innovative technologies such as underwater gliders are helping to obviate this issue (REF); there is great scope in addition for high-resolution regional modeling to aid understanding of key processes and the causes of change. Such models can also be used to diagnose the source and amount of freshwater injected into different areas of the WAP shelf, and to study the influence of different processes (e.g., wind mixing and freshwater-induced stratification) on MLD and other key ocean properties.

Surface MLD resolved by ocean models are often too shallow, especially in the Southern Ocean (Noh and Lee, 2008; Belcher et al., 2012; Schiller and Ridgway, 2013), and this bias has been attributed partially to the neglect of Langmuir circulation that results from the interaction between winds and surface waves (Belcher et al., 2012; D'Asaro, 2014). Langmuir circulation (LC) comprises a series of shallow vortices that counter-rotate on a vertical plane in the surface mixed layer. Strong velocity and vertical shear of the velocity in the Langmuir vortices enhance near-surface turbulence, erode stratification at the top of the thermocline, and thus deepen the surface mixed layer (e.g., Li et al., 2013).

How wind, waves and Langmuir-induced turbulence might affect MLD and mixing processes in the presence of an ice cover is an active area of research. Although the presence of a consolidated ice cover can greatly attenuate waves, a less consolidated ice cover, which typically characterizes WAP seasonal sea ice, can permit ocean waves to travel 100's of kilometers into the ice cover (e.g., Kohout et al., 2014; 2020/in review), potentially affecting sea ice growth processes (Doble et al., 2003), sea ice distributions (Kohout et al., 2014), sea ice melt and near-surface mixing processes (Smith et al., 2018). Other processes, such as air-sea flux and coastal freshwater input, could also affect the surface MLD.

As the first part of the Palmer-LTER modeling component to study biophysical and biogeochemical processes on the WAP shelf region, this study aims to understand how different physical factors affect surface MLD in the region, with a view to enabling subsequent works on biophysical and biogeochemical processes on the WAP shelf. To test the influence of LC on the MLD in the WAP region, this study tests two different parameterizations of LC, based on Li et al. (2017) and Li and Fox-Kemper (2017). While these parameterizations have been tested in global models, this is the first study to implement them in a regional Southern Ocean model. Simulations with different wind-ice drag coefficients are also analyzed to evaluate the influence of sea ice and wind mixing on the MLD at both seasonal and interannual time scales. The simulations are also compared to the available freshwater data (based on oxygen isotope analysis of surface seawater samples collected annually) to determine the relative impact of sea-ice production/meltwater and meteoric (glacial and precipitation) freshwater inputs in different areas of the WAP shelf (e.g., Meredith et al., 2017). Results highlight the critical need to correctly incorporate sea ice dynamics in order to properly simulate the ocean physics in the WAP.

## 2 Methods

### 2.1 Model and Grid Description

This study uses a hydrostatic version of the Massachusetts Institute of Technology General Circulation Model (MITgcm) and the embedded sea-ice and ice shelf modules. MITgcm solves Boussinesq Navier-Stokes equations with the hydrostatic assumption on Arakawa-C grid and z-level (fixed depth) vertical layers (Marshall et al., 1997a; 1997b). The sea-ice component of the model is based on Hilbler-type ice theromodynamics and elastic-viscous-plastic (EVP) ice rhelogy (Losch et al. 2010). The ice-shelf component (Losch, 2008) is also used here to include the freshwater input from ice shelf melt. MITgcm has been successfully used to resolve large-scale circulation, sea-ice dynamics and biogeochemistry of the Southern Ocean with horizontal resolutions on the order of a degree of latitude and longitude (Holland et al., 2014; Hauck et al., 2015; Taylor et al., 2013).

The model used in this study is a development of that presented in Regan et al. (2018). It covers a region ranging from 74.7˚S, 95˚W in the southwest to 55˚S, -55.6˚W in the northeast and includes the Bellingshausen Sea, the full extent of the WAP and the Drake Passage (Figure 1a). The model domain was chosen to extend from the southern Bellingshausen Sea (and includes also the southern ice shelves, the Wilkins and George VI ice shelves), to north across the Drake Passage to the southern tip of Chile. It therefore includes the Antarctic Circumpolar Current (ACC) that traverses this domain, flowing northeastward along the shelf break and affecting shelf break processes. The grid is curvilinear with 0.2 degrees of resolution for latitude and resolution varying between 0.0538 and 0.1147 degrees for longitude. Vertically, a z-grid (Losch et al., 2010) with 50 levels is used. The model bathymetry comes from the BEDMAP2 dataset (Fretwell et al., 2013), but is complemented with data from the General Bathymetric Chart of the Oceans (GEBCO, www.gebco.net) north of 60˚S, which is the northern extent of BEDMAP2.

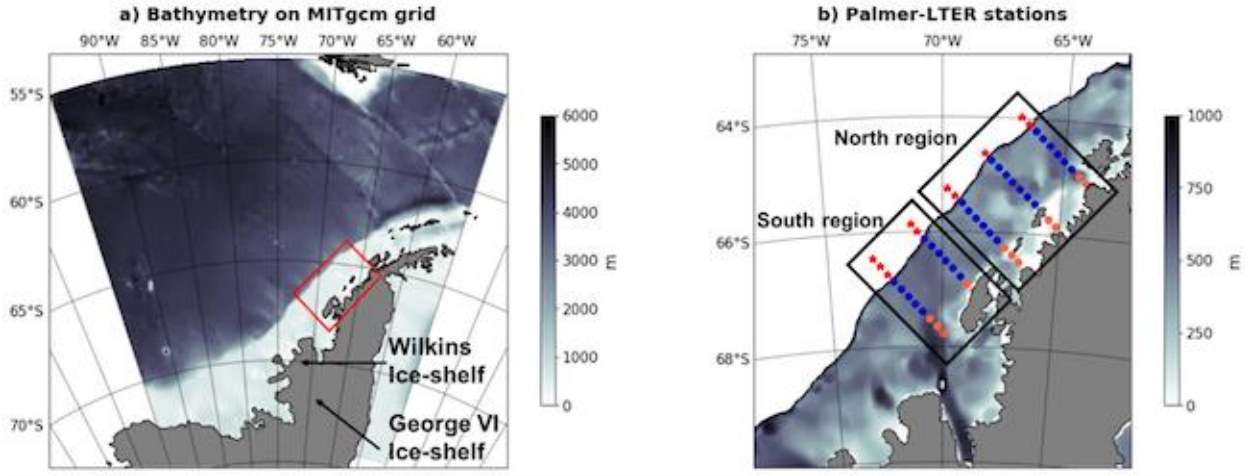


Figure 1: a) Model bathymetry with the region of Palmer-LTER cruises marked in the red rectangle and b) locations of the Palmer-LTER stations. Orange dots represent coastal stations, blue dots represent shelf stations, and red stars represent slope stations. The transect lines in the southern region are lines 200 (southernmost) and 300, and the transect lines in the northern region are 400, 500 and 600 (northernmost). Sub-regions analyzed are named northern coastal (n_cs), northern shelf (n_sh), northern slope (n_sl), southern coastal (s_cs), southern shelf (s_sh) and southern slope (s_sl).

## 2.2 Initial and Boundary conditions, and surface forcing

The initial conditions for temperature and salinity were obtained from the World Ocean Atlas (WOA, Boyer et al., 2009). The model has three open boundaries (north, east and west) with prescribed monthly mean ocean temperature, salinity and velocity, as well as sea-ice concentration, thickness and velocity obtained from a large-scale, low-resolution circumpolar MITgcm simulation (Holland et al., 2014). Sea-ice velocities are not prescribed at the boundaries to avoid spurious ice convergence. The atmospheric forcings are obtained from the ERA-Interim reanalysis (Dee et al., 2011) with a horizontal resolution of 1.5˚ in latitude and

longitude and a 6-hour interval. Although ERA-Interim has been found to be the most reliable reanalysis for some atmospheric parameters (Bracegirdle and Marshall, 2012), it is also known that most reanalyses, including ERA-Interim, underestimate moderate to high wind events.

As this model was originally used to study freshwater distribution in the Bellingshausen Sea, the freshwater inputs were carefully chosen to be as realistic as possible, given the constraints imposed by lack of data (Regan et al., 2018). A general surface runoff input was imposed to represent surface melt of land-based ice, and iceberg calving and melting. Values of the total surface runoff are chosen to represent the amount estimated by Van Wessem et al. (2016), and they are distributed uniformly along the coast and linearly decreasing with distance from land out to 100 km. Different from the steady freshwater input used in Regan et al. (2018), this study introduces a seasonal cycle of the freshwater input with greater values in summer and smaller values in winter. The annual mean glacial input was multiplied by a cosine anomaly in time, which gives a different value for each month and maintains the total input amount over the course of a year.

### 2.3 Parameterization of Langmuir Circulation

The model uses the K-profile parameterization (KPP; Large et al., 1994) to parameterize sub-grid scale vertical turbulence in the surface boundary layer and ocean interior, and here we consider the influence of LC in the KPP framework as an enhancement factor to the turbulence velocity scale used for the surface boundary layer. The time scale of ocean surface layer responding to winds, forming surface waves, and establishing/dissipating Langmuir vortices is relatively short (Talley et al., 2011). The impact of LC on mixing and surface MLD could thus be considered by directly coupling surface wave models with atmospheric conditions. However, direct simulation of the ocean surface waves over the spatial and temporal scale of our interests is computationally prohibitive, and there is limited data for validating wave models in the Southern Ocean. For this reason, this study employs empirical wave spectra, following Li et al. (2017), to estimate the surface wave conditions using winds at 10 m above sea surface.

Two approaches of including LC, based on the parameterizations of Li et al. (2017) and Li and Fox-Kemper (2017), respectively, are tested here. The approach described in Li and Fox-Kemper (2017) parameterizes the influence of LC in the entrainment of dense water from below the mixed layer. Two main factors affecting the rate of entrainment, i.e., entrainment buoyancy flux, $\overline{w'b'}_e$, are i) destabilizing surface buoyancy flux, important in convective turbulent regimes and ii) shear instability at the base of the surface mixed layer, dominant under wind-driven regimes. The latter factor is often associated with processes such as inertial oscillations of the surface current. Here, $w$' is vertical turbulent velocity anomaly, and $b$' is buoyancy fluctuation. When both factors are present, a proportionality is assumed and a new velocity scale, $w_x$, combining convective velocity scale and water-side friction velocity (Large et al., 1994), is introduced. $w_x$ relates to the rate of entrainment so that:

$$\overline{w'b'}_e = -0.2 w_x^3 / h_b$$

(Equation 1)

where $h_b$ is the boundary layer depth and is defined as the smallest depth at which the bulk Richardson number,

$$Ri_b(z) = \frac{|z|[b_r - b(z)]}{|u_r - u(z)|^2 + U_t^2(z)}$$

(Equation 2)

reaches a critical value of 0.3. Here, $u_r$ is a reference speed, $u$ is water speed, $b_r$ is a reference buoyancy, $b$ is buoyancy, and $U_t$ is a velocity scale that accounts for the influence of subgrid velocity and shear. Several large-scale eddy simulations (e.g., Grant and Belcher, 2009; McWilliams et al., 2014) have suggested that $\overline{w'b'}_e$ is enhanced in the presence of LC. This would happen because LC enhances turbulent kinetic energy (TKE) at the base of the mixed layer. Langmuir turbulence could also contribute to the erosion of the thermocline through enhancing shear instability beneath the downwelling regions of the LC cells. However, quantifying the Langmuir enhanced $\overline{w'b'}_e$ is nontrivial due to small magnitude of the TKE budget as a whole.

The solution proposed by Li and Fox-Kemper (2017) includes the introduction of a new velocity scale, $U_t$, based on the surface turbulent Langmuir number:

$$U_t(z) = \frac{C_v\, N(z)\, w_s(z)|z|}{Ri_c}\left[\frac{-\overline{w'b'}_e h_b}{w_s(z)^3}\right]^{-1/2}$$

$$= \frac{C_v\, N(z)\, w_s(z)|z|}{Ri_c}\left[\frac{0.15w^{*3} + 0.17u^{*3}(1 + 0.49La_t^{-2})}{w_s(z)^3}\right]^{-1/2}$$

(Equation 3)

where $N$ is the local buoyancy frequency, $w_s$ is the turbulent velocity scale, $C_v$ is a defined parameter based on buoyancy, $u^*$ is the magnitude of frictional velocity, $Ri_c$ is the critical Richardson number, $La_t$ is the turbulent Langmuir number:

$$La_t = \sqrt{u^*/u_0^s}$$

(Equation 4)

and $u_0^s$ is the Stokes drift speed, which is the average speed of a specific fluid parcel over multiple wave periods. While the Stokes drift is not calculated by the model, it is dependent on the high-frequency part of the wave spectrum, which is reasonably well described by the empirical wave spectra. The wave spectra used to calculate the Stokes drift is based on the Phillips spectrum (Phillips, 1985), and the directional spreading of wind waves of Webb and Fox-Kemper (2015) is also considered. In the calculation of wave spectra, the peak frequency is

often assumed to be related to the wind speed, so that the wind speed at 10 m height is used for this calculation.

The second approach tested in this study, based on the work of Li et al. (2017), represents Langmuir turbulence as an enhancement factor applied to the turbulent velocity scale used in the KPP formulation. The idea of an enhancement factor had already been presented by McWilliams et al. (2000), whose enhancement factor is a function of $La_t$. However, the formulation proposed by McWilliams et al. (2000) introduces spurious extra mixing in the extra-tropical regions, possibly because it does not include wind-wave misalignment. The parameterization of Li et al. (2017) uses a theoretical wave model based on the Stokes drift profile, the boundary layer depth and the surface friction velocity (see equation 25 of Li et al., 2017):

$$\varepsilon = f(u_{10}, u^*, \hbar_b) \quad \text{(Equation 5)}$$

where $u_{10}$ is the wind velocity at 10-meters height. The boundary layer depth and surface friction velocity are provided by the model, and the Stokes drift is calculated as previously explained.

Both parameterizations of LC depend on wind speed and assume direct work of wind on the ocean surface. However, the presence of sea ice modifies ocean surface waves and the air-ocean drag, which in turn modifies the surface momentum exchange (Andreas et al., 1984; Birnbaum and LÜpkes, 2002). The efficiency of wind inducing Stoke drift thus varies with sea-ice concentration (SIC). Here, to consider the influence of sea ice on the wind work, we seek to introduce a coefficient to the 10-m wind speed. While there are no data or concrete formula to describe the change of wind work around sea ice, a study by Andreas et al. (2010) using data collected in the Arctic over a year-long experiment proposes a relationship between SIC and *Cd*, the drag coefficient of the friction between 10-m wind and ocean:

$$10^3 Cd = 1.5 + 2.233 \times SIC - 2.333 \times SIC^2 \quad \text{(Equation 6)}$$

It is seen from this equation (plotted on supplemental material) that *Cd* is enhanced at intermediate SIC. This can be explained by the fact that at low to intermediate SIC ice floes will have higher pressure in the upwind and lower pressure in the downwind face, essentially functioning like a sail, which enhances the wind work. At high SIC, ice floes shelter each other and decrease the momentum transfer from air to the ocean. Since frictional velocity is proportional to *Cd*, we assume that the quadratic dependence of *Cd* on SIC can be translated to the dependence of Stokes velocity on SIC. Therefore, we derived an equation for an enhancement factor ($s_c$) dependent on SIC to be multiplied by the wind velocity, $U_{10}$, and account for increased momentum transfer at intermediate SIC:

$$s_c = 1 + 2 \times SIC - 3 \times SIC^2 \quad \text{(Equation 7)}$$

so that $s_c$ (plotted against SIC in supplemental material) equals one in the absence of sea ice (no enhancement), peaks at intermediate concentrations and at a rate similar to the *Cd* enhancement (~35%), and is zero when SIC approaches one (no Langmuir influence in areas completely covered by sea ice due to absence of ocean surface waves). There are great uncertainties in this relationship between wind influence and SIC, and the uncertainties are at the moment impossible to be clarified due to the lack of data. Nevertheless, we assume this approach of considering sea ice influence on the LC is more realistic than using a linear relationship between wind influence and SIC.

2.4 Description of experiments

Hindcast simulations were integrated between 1984 and 2014, with 1984 to 1990 considered spin-up. Therefore, the model period analyzed covers the period from the beginning of the Palmer-LTER field measurements (1991 onwards, see section 2.5) until 2014. The model output consists of daily averages of the ocean and sea-ice variables. The study examines four simulations with different parameterizations for LC and different values for air-sea-ice drag coefficient, *Cd* (Table S1 on supplemental material).

The value of *Cd* is linked to the characteristics of sea ice and shows a wide range of values in both observational and modeling studies, ranging from $5 \times 10^{-4}$ to $>3 \times 10^{-3}$ (e.g. Wamser and Martinson, 1993; Castellani et al., 2014; Miller et al, 2006; Tsamados et al., 2014). The value used in Regan et al. (2018) was $5 \times 10^{-4}$, on the lower end of Cd estimates. The choice of using a low *Cd* value was intended to adjust the formation of polynyas around Eltanin Bay (south of the Palmer-LTER region) and the freshwater fluxes around George VI Ice Shelf. Lowering the drag coefficient also lowers the impact of wind in transporting sea ice to different regions, hence curbing the formation of polynyas. For the Palmer-LTER region, however, a lower drag coefficient means that more sea ice could be melted locally rather than be transported elsewhere, thus lowering the surface salinity and increasing stability in coastal and shelf regions. Therefore, *Cd* values of $5 \times 10^{-4}$ and $2 \times 10^{-3}$ (on the higher end of the observed values) were used in different simulations to assess the impact of sea-ice transport in local surface ocean mixing and freshwater budget.

In the control simulation (CTRL), *Cd* = $2 \times 10^{-3}$ and the parameterization for LC is based on the entrainment buoyancy flux (Li and Fox-Kemper, 2017). Sensitivity simulation LowCd has a similar configuration to CTRL, but with *Cd* = $5 \times 10^{-4}$. To assess the effect of different parameterizations for LC, sensitivity simulations without any LC parameterization (NoLC) and with the LC parameterization based on an enhancement factor for wind mixing (EnhLC; Li et al, 2017) are carried out. All other parameters in NoLC and EnhLC are the same as in CTRL.

## 3 Data used for skill assessment

The Palmer-LTER project started in 1991 and has been collecting a range of physical, biological and chemical data along the WAP since, including semiweekly water-column sampling from Palmer Station from October through March each year and an annual cruise each January-February since 1993 (Ducklow et al., 2013). Given that the data collected at Palmer Station are highly influenced by local phenomena, such as the passage of icebergs, that are not captured by the model, they are excluded in the model validation and analysis.

The cruise data used for model validation are from lines 200 to 600 of the Palmer-LTER grid, spanning an area of 500 km along the coast and 250 km across the shelf. The cross-shelf transects are spaced every 100 km in the along-shelf direction, and the stations on each transect are separated by 20 km (figure 1b). All the data collected are available through the project web page (http://pal.lter.edu/data/). Modeled vertical profiles of salinity and temperature are compared to the cruise CTD (conductivity, temperature and depth) profiles. It is important to note, however, that not all stations are sampled every year.

Each individual CTD cast does not necessarily reflect the mean state of the water column during the summer of data collection due to the influence of synoptic processes. In order to decrease the influence of short-term and small-scale processes on the CTD casts during the analyses, the cruise data are divided in north (lines 400, 500 and 600) and south (lines 200 and 300) regions (Figure 1b), and also into coastal, shelf and slope regions, based on topography. This way, 6 different sub-regions are obtained: north coastal (n_cs), north shelf (n_sh), north slope (n_sl), south coastal (s_cs), south shelf (s_sh) and south slope (s_sl).

Onset time of sea-ice advance and retreat are obtained from the GSFC (Goddard Space Flight Center) Bootstrap algorithm (Comiso, 2017). The sea-ice year starts in mid-February, from day 46 of the calendar year until day 410. SIC refers to the percentage of each cell area covered by sea ice, ranging from zero (no sea-ice cover) to one (totally covered by sea ice). Onset time of sea-ice advance is chosen to be the day in which the average SIC of all the stations in each Palmer-LTER grid sub-region reaches at least 0.15 for 5 days in a row. Onset time of sea-ice retreat is calculated as the last day in which SIC is less than 0.15 for the sea ice season. Further details are provided in Stammerjohn et al. (2008; 2012). The sea-ice data used to calculate the climatological SIC for each sub-region is from the same source, and binned as 8-day means with horizontal resolution of 0.2 degrees in both latitude and longitude. For surface freshwater content, oxygen isotope data, described in Meredith et.al. (2008, 2010, 2013) was the primary dataset used for the model skill assessment.

# 4 Results

To compare the model results with the Palmer-LTER cruise data, values at model grid points closest to Palmer-LTER stations are analyzed. Following Mitchel and Holm-Hansen (1991), we use the threshold of density change of 0.05 kg/m$^3$ over a 5-meter interval to define surface MLD. Onset times of sea-ice advance and retreat in the model data were calculated as per the observational data.

As a first assessment of the skill of the model in reproducing the broad seasonal patterns observed in the surface ocean in the WAP region, we examine summer (December to February) and winter (June to August) climatological surface salinity, temperature, currents and SIC in Simulation CTRL (figure on supplemental material). The main circulation pattern in the WAP region is a northeastward current of the ACC along the shelf break, which is present in the model results. The horizontal resolution of the model is not sufficient to properly resolve the coastal circulation, described in Moffat and Meredith (2018), however the outputs do capture the cross-shelf flows described in the same study. The modeled sea surface temperature (SST) shows an onshore-offshore gradient during the summer, with colder waters on the shelf where sea ice has recently melted, as well as a latitudinal gradient with colder waters towards the southern part of the domain. During the winter, SST values reflect the sea-ice freezing temperature near the coast and shelf region in most of the area.

Simulation CTRL captures an onshore-offshore gradient in summer surface salinity with lower salinities reaching minimums of around 32.5 near the coast, as described in the literature (Meredith et al., 2017). While a salinity gradient is present in the winter in the southern part of the model domain, it is not as marked as during the summer months, when sea-ice melt and increased glacial input contribute to lowering the salinity near the coast. Sea ice extends past the shelf break during the winter and is confined to the region south of Marguerite Bay during the summer. Overall, seasonal variations of the surface variables in Simulation CTRL match the main patterns captured by the observations.

## 4.1 Sea-ice advance and retreat

To assess how well the model captures sea ice interannual variability, modeled onset times of sea ice advance and retreat over the simulation period are plotted against the observations (Figure 2). Correlation coefficients between modeled and observed onset times of sea-ice advance and retreat for each sub-region are calculated (Tables S2 and S3 on supplemental material). When comparing the results of the CTRL simulation with the observations, it is seen that sea-ice advance is well represented in the model in the southern region, while in the north the model shows earlier advance in the coastal and shelf areas. For sea-ice retreat, the CTRL run performs better in the shelf and slope regions than in the coastal

regions. In the northern coastal region, the model shows earlier retreat than the observations in most years, and while in the southern coast the model was able to capture the timing of sea ice retreat observed, years of early (2006, 2007, 2010) and late (2004) retreat were not well represented.

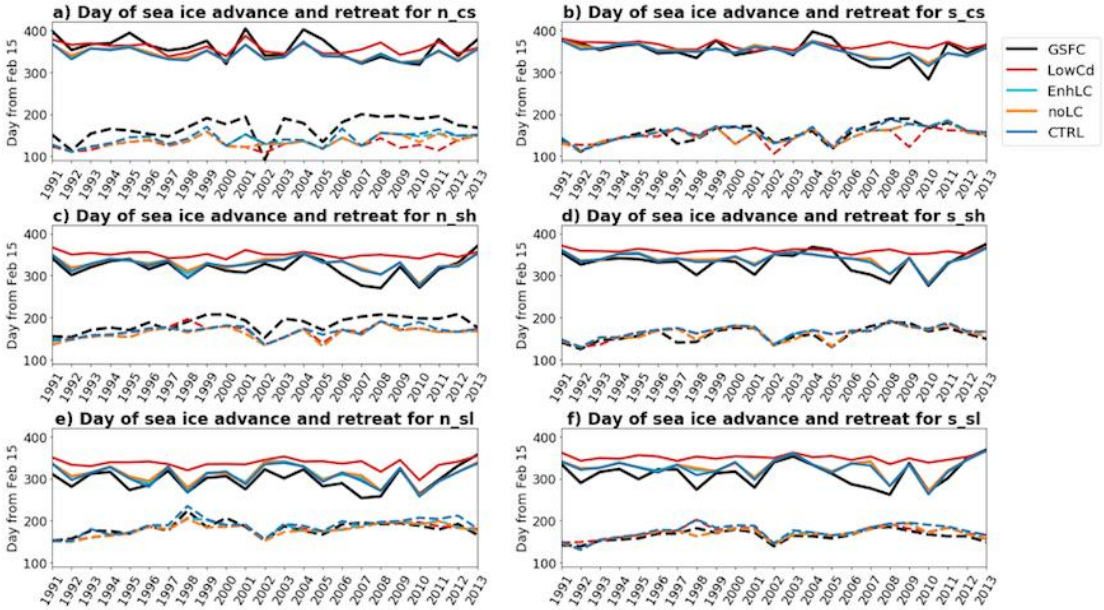


Figure 2: Evolution of the onset times of sea ice advance (dashed line) and retreat (solid) in sub-regions northern coastal (a), southern coastal (b), northern shelf (c), southern shelf (d), northern slope (e) and southern slope (f). Black lines represent results for satellite observations, and other lines represent results from different simulations.

Wind action has a larger influence in the timing of sea-ice advance and retreat than LC, evidenced by the larger difference between the CTRL and LowCd results compared to the difference between CTRL and EnhLC/noLC. The comparison simulations suggest that wind action has a larger influence on the retreat of sea ice than on the advance. This likely reflects the fact that sea ice advance is driven more by thermodynamics rather than mechanical forcing. The influence of LC on sea-ice advance/retreat was much more modest and mainly consisted of small differences in the onset time of sea-ice advance. Without any parameterization for LC (NoLC) sea ice advances slightly earlier in the coastal areas, and in the slope region in some years.

Interannual variability of the timing of sea-ice advance and retreat also seem to be more influenced by wind action than by representation of LC. The correlations between modeled and observed sea-ice advance and retreat show that the CTRL simulation has better representation of interannual variability, with correlation coefficients mostly higher than 0.8, with the exception of sea-ice advance in the northern coast (0.62) and shelf (0.70) regions. The coefficients calculated for experiments EnhLC and NoLC were similar to those of the CTRL run, and LowCd had the lowest correlations for both sea ice advance and retreat.

In summary, the choice of wind-sea-ice drag coefficient has a larger impact in the representation of seasonal and interannual sea-ice cycles than the inclusion of LC, with low drag leading to higher SIC and delayed sea-ice retreat. While sea-ice retreat seems to be highly affected by wind influence on sea ice, differences in sea-ice advance do not seem to be related to wind in all regions except for northern coastal, and are likely more affected by changes in surface salinity and temperature between the simulations. Biases in atmospheric forcing (particularly wind forcing) might play a role in the disparities found between the models and observations in some years, and their exact contribution and the associated mechanism are unclear and left for future studies.

## 4.2 Surface Mixed Layer Depth (MLD)

### 4.2.1 Variability of Summer MLD

In order to compare the model results to the Palmer-LTER CTD cruise data, simulated daily MLD in each sub-region in the months of January and February are averaged for each year. The results are compared to the observed mean MLD in each sub-region for each cruise (Figure 3). The choice of using the modeled mean MLD in January and February was made because January and February are the months in which the cruises (which last about 6 weeks) take place. Comparing the results on individual dates would not necessarily improve the model-observation comparison, since small scale phenomena such as passage of submesoscale features and icebergs or a locally-strong wind might affect the MLD at each individual station, and these phenomena are not captured by the model. However, with a long enough dataset, and using data from different stations, the Palmer-LTER cruise data should be able to represent the interannual variability of MLD in the WAP to some degree at regional scale.

The CTRL simulation gives mean MLD shallower than observed throughout the domain. The difference between model and observations is particularly large in the southern coastal and northern shelf regions. Although less variation is expected in the modeled MLD, given it is represented as a 2-month average, it also shows lower standard deviation (calculated from daily values). However, the interannual variability in the CTRL simulation seems to be reasonably well represented in most of the domain, with correlation with observation greater than 0.93 in the southern shelf. Modeled MLD variability is less representative in the northern coastal (correlation = 0.308) and southern slope (correlation = 0.110) regions. The low correlation in the northern coast is expected as MLD in the coastal region is influenced by local phenomena that are not well captured by the model. It is not clear why the southern slope fails to capture interannual variability. A possibility is that the southward advection of sea ice during the retreat is less pronounced in the model compared to observations, which would affect the amount of melt in the southern slope. Although there is limited data on sea-ice thickness, it is also possible that it is overestimated in the model.

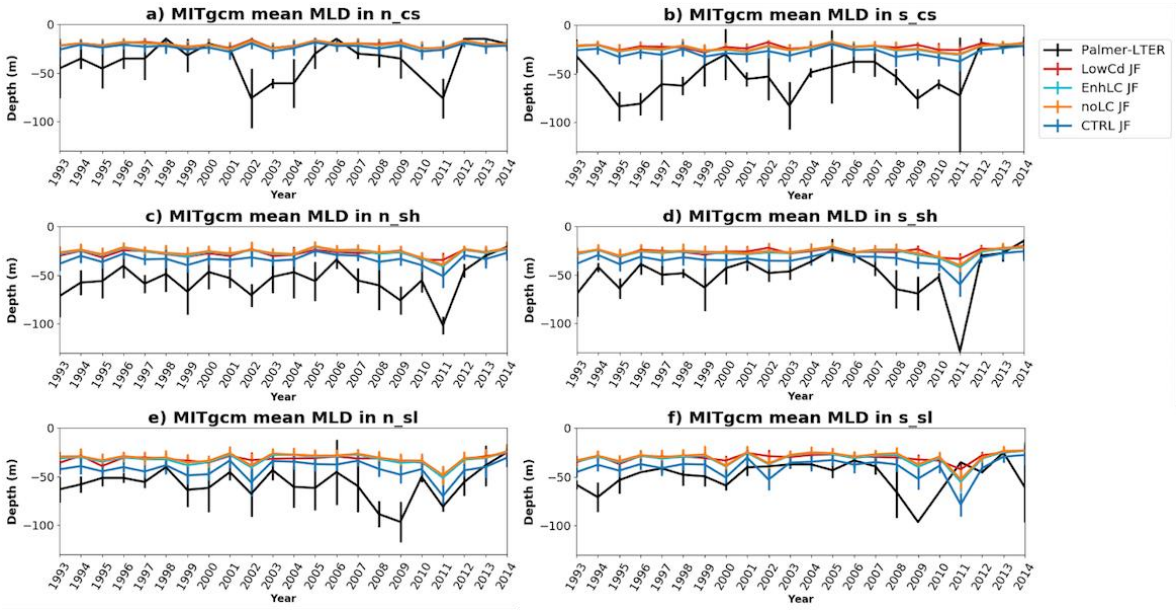


Figure 3: Averaged mixed layer depth (MLD) for January and February each year from the Palmer-LTER cruise (black lines) and from the simulations (other colors). For the model data, vertical lines indicate the standard deviation of the data considered in each sub-region and year; for the Palmer-LTER data, vertical lines represent the standard deviation of the data in each sub-region for each cruise. Data are shown for northern coast (a), southern coast (b), northern shelf (c), southern shelf (d), northern slope (e) and southern slope (f).

The CTRL simulation had the deepest MLD among all the sensitivity simulations. Despite having the same parameterization for Langmuir circulation as CTRL, LowCd MLD was mostly similar or shallower than NoLC and EnhLC, implying that properly representing wind-sea-ice drag in the model has as much or more influence on MLD as properly representing Langmuir circulation. Between the two approaches to parameterizing LC, entrainment from the bottom of the mixed layer (CTRL) had a larger impact than applying an enhancement factor (EnhLC).

Overall, the CTRL simulation had better performance in simulating both the depth and interannual variability of the mixed layer, although a bias towards shallow MLD still persists. This indicates that both using a higher drag coefficient and including LC parameterization based on entrainment buoyancy flux are important for resolving the MLD, but properly simulating the sea-ice cycle as well as capturing the redistribution and volume of sea ice melt have a bigger impact in reproducing the interannual variability of the MLD.

### 4.2.2 MLD seasonality

Although seasonality of MLD is hard to validate due to lack of data during the cold months of the year, it is known that MLD deepens during the winter due to surface cooling, formation of sea ice and subsequent brine rejection. Comparisons between the seasonal cycle of MLD in the different model simulations were made to investigate how the changes made to the model parameters affect MLD throughout the year. For that purpose, the monthly

climatology of MLD for each sub-region was plotted for all model simulations (Figure 4). Immediately apparent from the figure is that the CTRL simulation has deeper MLD throughout the year and in all sub-regions, with maximum depth being reached in August and deeper MLD farther away from the coast.

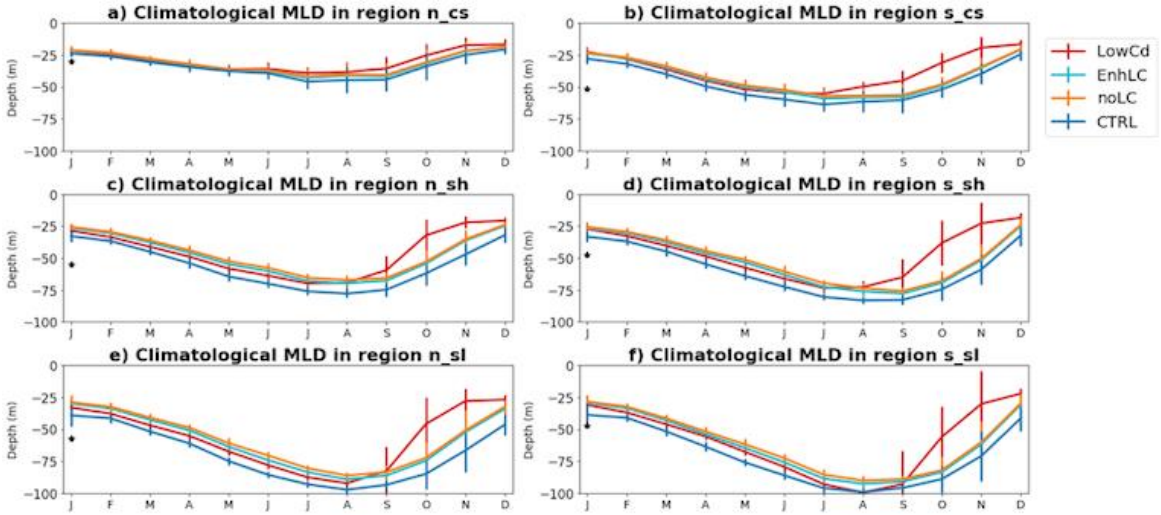


Figure 4: Simulated monthly climatologies of MLD in northern coast (a), southern coast (b), northern shelf (c), southern shelf (d), northern slope (e) and southern slope (f) regions. The black star in January represents the average observed MLD for each region, calculated using the Palmer-LTER cruise data.

LowCd has consistently shallower MLD, except for the month of August in the southern slope region. The difference between these two simulations is more accentuated during the spring and early summer, when LowCd overestimates SIC (supplemental material). Shallower MLD in LowCd occurs even in areas and months in which sea ice is absent and both simulations would have similar physics. Regarding the different parameterizations of LC, applying the enhancement factor (EnhLC) only seems to deepen the mixed layer during the fall and winter in the slope regions, when the difference between EnhLC and noLC is visible but smaller than 5 meters. The parameterization used in the CTRL simulation, based on entrainment from below the mixed layer, deepened the MLD throughout the domain with the exception of summer and fall in the northern coast. From the results, we conclude that increased SIC during the spring and summer will shoal the MLD during these seasons, and in this case a shallower MLD can also be seen during fall and winter in most regions. Properly simulating sea-ice retreat, therefore, is important for the simulated MLD year-round.

### 4.3 Vertical structure of the water column

The water mass distribution in the surface and subsurface layers of the WAP are marked by the presence of Antarctic Surface Water (AASW), Winter Water (WW) and Circumpolar Deep Water (CDW), respectively, and have been described in several studies (e.g. Klinck et al. ,2004;

Moffat et al., 2008; Moffat and Meredith, 2018). CDW is a subsurface water mass derived from the Antarctic Circumpolar Current (ACC), which flows close to the shelf break at the WAP, sporadically intruding onto the shelf. CDW is comparatively warm, with temperatures higher than 1˚C, and nutrient rich, playing an important role for primary production. CDW is modified as it flows across the shelf, cooling linearly with distance towards the coast. Above the CDW is the WW, which is formed by deep mixing from brine rejection during winter sea ice production, which then becomes isolated (forming 'remnant WW') from the surface by summer stratification. The summer surface stratification is due to increased heat input from solar radiation and freshening during sea-ice melt and glacial discharge from land, forming the AASW, which consequently traps the remnant WW between the AASW and the modified CDW, and is represented by a cold layer (temperatures below 1˚C) located between 80 to 100 meters.

The mean January/February salinity and temperature profiles of each model experiment were plotted for each sub-region along with the average Palmer-LTER cruise profile (Figure 5 for northern region and Figure 6 for southern). The August averages for each experiment are also plotted to represent the winter water column (supplemental material). The vertical profiles of the CTRL simulation have lower surface salinity and higher surface temperature when compared with the summer observations, which is consistent with late and increased sea-ice melt. An increased amount of meltwater would lower surface salinity and increase the stability of the surface layer. With a more stable surface layer, heat from the atmosphere is distributed over a shallower depth, increasing the surface temperature and further increasing the stability of the mixed layer. In the observations, a deeper mixed layer leads to lower surface temperature not only because surface heat is distributed deeper, but also because more WW is entrained from below.

Compared to the CTRL simulation, LowCd has lower surface temperature and salinity during the summer, likely because sea-ice retreat happens later in LowCd. New meltwater on the surface tends to be cold prior to gaining heat through insolation. Although LowCd brings the surface temperature closer to observations when compared to CTRL, this likely happens for the wrong reason: due to late sea-ice retreat, instead of deeper mixing. During the winter, salinity profiles are similar between the simulations in the slope region, but LowCd shows lower surface salinity in the coast and shelf.

At the surface, the simulation with no LC shows higher temperature and lower salinity in the summer compared to CTRL, increasing the differences from the observations and confirming the positive impact of buoyancy flux entrainment-based LC parameterization on properly simulating the surface ocean layer. Using the enhancement factor to parameterize LC (EnhLC) had similar results to the simulation with noLC. The only difference observed between EnhLC and noLC during the summer is a slightly lower salinity close to the surface in EnhLC. Although EnhLC had larger impact on vertical salinity and temperature during the winter when

compared to noLC, the effect of the enhancement factor was still smaller than the parameterization included in the CTRL simulation.

The differences observed in MLD and vertical profiles among the simulations suggest that the influence of late and increased sea-ice melt in the coastal and shelf region during the summer persists throughout the year, with lower surface salinity and shallower mixed layer observed during the winter. On the slope, winter MLD is more impacted by the choice of LC parameterization than by the choice of drag coefficient.

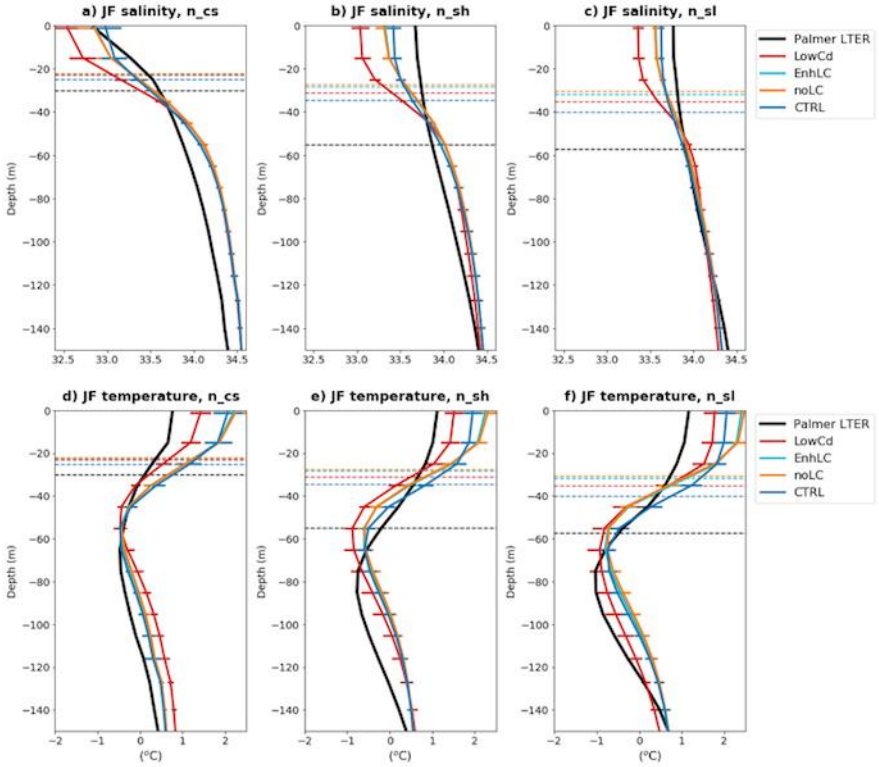


Figure 5: Simulated January-February climatology and Palmer-LTER cruise climatology of salinity for (a) northern coast, (b) northern shelf and (c) northern slope regions; and simulated January-February climatology and Palmer-LTER cruise climatology of temperature for (d) northern coast, (e) northern shelf and (f) northern slope regions. Horizontal solid lines represent standard deviation, and horizontal dashed lines indicate climatological MLD for the period considered.

### 4.4 Freshwater seasonality

The freshwater cycle in the WAP has an important role for the coastal circulation (Moffat et al., 2008; Moffat and Meredith, 2018) and for primary production. Glacial meltwater, in particular, is thought to be a major source of dissolved iron (Annett et al., 2017), which is likely the limiting nutrient in the WAP given that nitrogen and silica are rarely depleted (Kim et al., 2016). Studies aimed at quantifying the amount and source of freshwater in the WAP surface ocean have been conducted using oxygen isotope data (Meredith et al., 2008; 2013; 2018) to identify whether the freshwater is derived from sea-ice melt or from meteoric sources,

which is derived from the atmosphere and includes precipitation and glacial melt. Although sea-ice formation and melt does not represent a net input of freshwater if integrated over a full season and over a large enough region, an excess of sea-ice melt (formation) can be a source (sink) of freshwater at certain locations due to the redistribution of sea ice (i.e., by winds) from the location where in situ growth occurred.

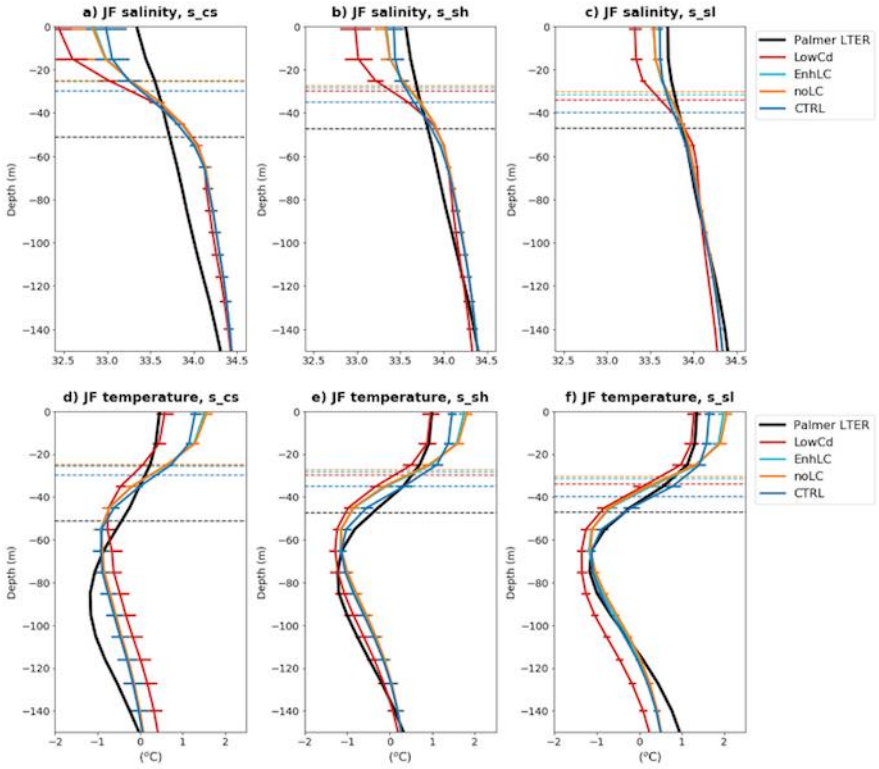


Figure 6: Simulated January-February climatology and Palmer-LTER cruise climatology of salinity for (a) southern coast, (b) southern shelf and (c) southern slope regions; and simulated January-February climatology and Palmer-LTER cruise climatology of temperature for (d) southern coast, (e) southern shelf and (f) southern slope regions. Horizontal slide lines represent standard deviation, and horizontal dashed lines indicate climatological MLD for the period considered.

Since the oxygen isotope samples were collected during the Palmer-LTER cruises in January and February, the spatial and temporal patterns of freshwater distribution derived from these data represent the summer distribution only. Given the model used in this study has a reasonable representation of the sea-ice cycle and includes seasonality in the discharge of glacial freshwater, the results can be used to estimate the influence of different sources of freshwater throughout the year. However, because there is no interannual variability in the glacial runoff in the model, the analysis is restricted to the seasonal climatology of freshwater.

From the cruise observations in late summer, it is seen that there is a cross-shelf gradient in salinity, with lower salinities around 33.2 near the coast coinciding with higher concentrations of meteoric water (Meredith et al., 2013). Although meteoric water has a highly variable and heterogeneous spatial distribution, cruise measurements indicate that it is the

dominant source of freshwater across the shelf in most years. Sea-ice melt concentrations in the near surface were highly variable from year to year (Meredith et al., 2017). Despite the high variability, the data also suggests that there is more sea-ice formation towards the north and more sea-ice melt towards the south of the WAP. Sea-ice formation, however, leads to deepening of the mixed layer, and the isotopic signature associated with this process also gets mixed downward in the water column during this process. Accordingly, there is a seasonal asymmetry in the vertical distribution of isotope-derived freshwater prevalences, which adds complexity to the interpretation of these data (Meredith et al., 2013).

To analyze the seasonality of the modeled freshwater sources in the different sub-regions, modeled climatological monthly means for sea-ice melt and meteoric freshwater are plotted for CTRL and LowCd (Figure 7), with positive values indicating addition of freshwater by sea-ice melt and negative values indicating sea-ice formation. The results of EnhLC and NoLC are not included in the figure because the sea ice cycle in those simulations is very similar to the CTRL simulation. Also, only one line is represented for meteoric freshwater, the sum of precipitation and glacial runoff, because the value is the same for all the simulations.

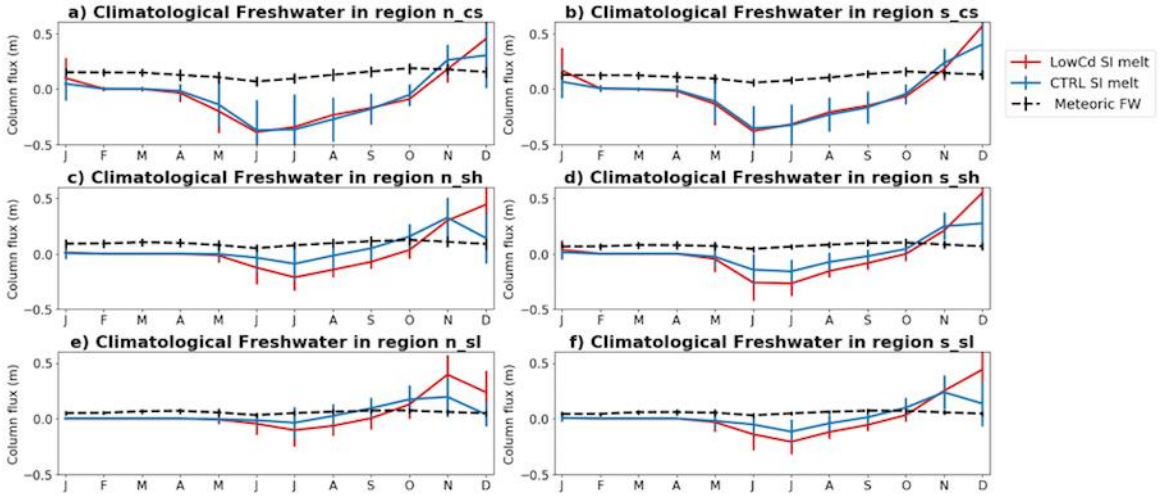


Figure 7: Monthly climatologies of sea ice meltwater (color) from Simulations LC (blue) and LC_Cd (red), and monthly climatology of simulated meteoric freshwater from the simulations (black) in northern coast (a), southern coast (b), northern shelf (c), southern shelf (d), northern slope (e) and southern slope (f) regions. Vertical lines represent the standard deviation.

It is seen that although a strong seasonal cycle is included in the glacial runoff, with increased discharge during the summer, seasonality in overall meteoric freshwater input is dampened by the precipitation in the atmospheric forcing. Meanwhile, a pronounced seasonal cycle exists in the sea-ice melt. The CTRL results for sea-ice melt indicate that it is the dominant freshwater source between October and December in some sub-regions. Towards the end of the summer meteoric water is present in higher concentrations throughout the whole domain, in accordance with the observations. CTRL results also show that most of the sea ice formation happens in the coastal region during the winter. Despite melt seasonality being different for

each sub-region, the overall summer melt, as indicated by the sum of sea-ice melt from October to February, is larger in the southern region for coastal (0.6 m north, 0.7 m south), shelf (0.47 m north, 0.53 m south) and slope (0.23 m north, 0.37 m south) stations, consistent with the observational result of more sea-ice melt in the southern region.

Sea-ice melt happens first in the northern region and in the slope, and progresses towards the south and coast. While this progression is observed in the CTRL simulation, LowCd sea-ice melt peaks in December in every sub-region with the exception of the northern slope, where melt peaks in November. The largest differences in sea-ice melt between CTRL and LowCd are found at the coastal stations in January, where the largest differences in surface temperature and salinity are also observed between these two simulations. The increased melt in the LowCd simulation during the summer confirms the hypothesis that the lower surface temperatures seen in the LowCd experiment (compared to CTRL) are due to recently melted sea ice.

Maps of climatological summer (December to February), winter (June to August) and annual meteoric, net sea-ice melt and total freshwater were also plotted for the CTRL simulation (Figure 8). It provides a broader assessment of the freshwater distribution throughout the WAP region. The observed onshore-offshore gradient in meteoric water is present in the summer and also seen in the annual values. The summer sea-ice melt values are larger towards the coast and southern region, in agreement with the observations. These high-melt areas are also areas of high sea-ice formation during the winter. The annual net sea-ice melt values, then, suggest net sea-ice formation near the coast and in Marguerite Bay, while higher net sea-ice melt is seen in the northern shelf. Since the freezing signal is dampened in the in-situ data due to vertical mixing, it is possible that the overall influence of sea ice melt is overestimated towards the south given data is collected during the months of highest sea-ice melt in that region.

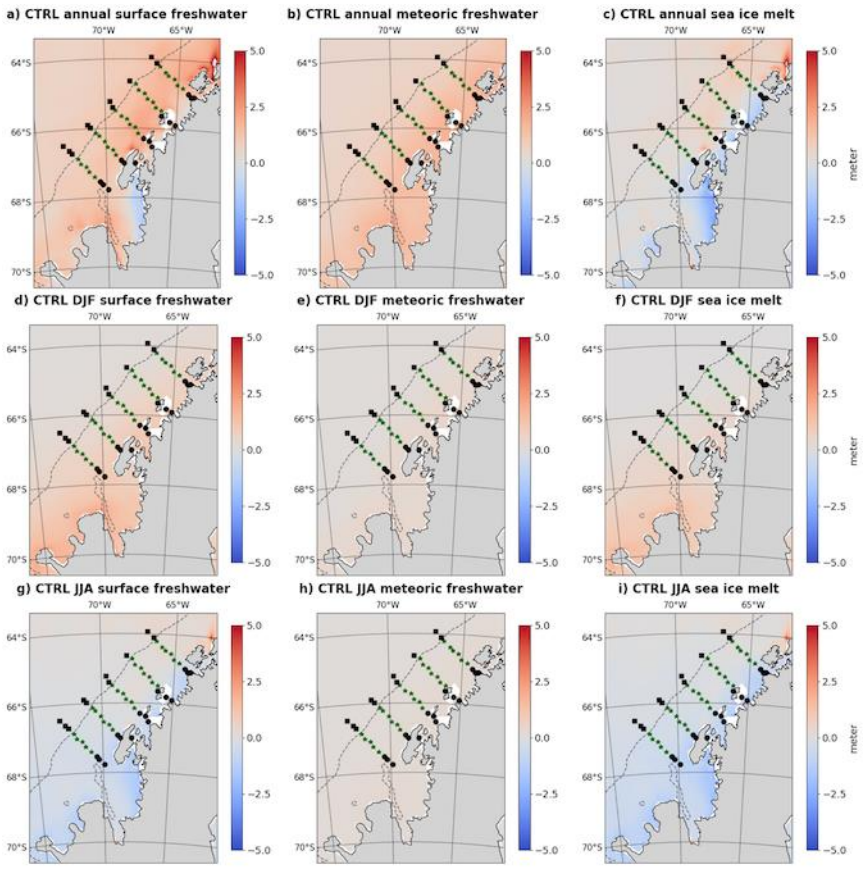


Figure 8: Annual climatology of fluxes (top row) of total freshwater (left column), meteoric freshwater (middle column) and sea ice melt (right column); summer (December-February) climatology of fluxes (middle row); and winter (June-August) climatology of fluxes (bottom row). Dashed lines represent 750-m isobath, taken to be the edge of the continental shelf, and the different symbols represent coastal (black dots), shelf (green) and slope (black diamonds) stations.

## 5 Discussion and Conclusion

Different ocean-sea ice hindcast simulations were conducted for a region encompassing the West Antarctic Peninsula (WAP) with different choices of wind-sea ice drag coefficient and parameterizations for Langmuir circulation to assess the effects of wind mixing and sea ice in the seasonal and interannual representation of MLD and freshwater cycles. Two different approaches to parameterizing Langmuir circulation were tested, based on the studies of Li et al. (2017) and Li and Fox-Kemper (2017). These approaches were applied to the KPP mixing parameterization and, respectively, include a Langmuir circulation-based enhancement term for wind mixing throughout the ocean surface mixed layer (Li et al., 2017) and a change in the vertical velocity scale in the critical Richardson number to increase entrainment of subsurface water from below the mixed layer (Li and Fox-Kemper, 2017).

We found that while the choice of LC parameterization does not significantly change simulated sea ice, the choice of wind-sea-ice drag coefficient lead to large differences in the representation of seasonal and interannual sea-ice variability. Since models are built to represent realistic physics, the model sensitivity to different parameterizations helps to

understand the influence of the processes parameterized in the real ocean. Therefore, this study implies that while wind action has a large impact on sea-ice cycle, the role of LC in driving sea-ice variability is limited. The CTRL simulation, which has a higher drag coefficient ($2 \times 10^{-3}$), shows a bias towards higher SIC and late sea-ice retreat when compared to the observations. These biases are amplified in the simulation with low ($5 \times 10^{-4}$) drag coefficient. The difference between simulations with different drag coefficients is much larger during the period of sea-ice retreat than during sea-ice advance, suggesting retreat is more influenced by wind action. The small differences in SIC during sea-ice advance can potentially be explained by thermodynamic effects. The sea-ice freezing temperature is higher for low-salinity waters, and earlier sea-ice advance is seen in simulations with lower surface temperature and salinity.

Both sea ice and LC impact the MLD in the WAP. The influence of sea ice on surface MLD it larger in the coastal and shelf regions, while the importance of LC for the MLD is larger than that of sea ice close to the sea ice margins (slope) during the winter. Shallower spring and summer MLD in the experiment with low drag coefficient (compared to CTRL) leads to shallower MLD in the fall and winter despite this experiment having similar physics to the CTRL simulation in the ice-free months, suggesting a lasting effect of improperly simulating summer sea ice.

A bias towards MLD being shallower than that observed has been seen in several modeling studies. For the LC parameterization, the mixed-layer entrainment approach proposed by Li and Fox-Kemper (2017) proved to be more effective in deepening the MLD than using an enhancement factor for wind mixing. Although the CTRL simulation includes the parameterization of Li and Fox-Kemper (2017) and a higher wind-sea-ice drag coefficient, the CTRL simulation still shows a bias towards shallow MLD compared to observations despite being the best performing simulation and being able to better capture interannual variability. While the interannual variability of MLD was reasonably simulated in most of the domain, the model failed to properly capture it in the northern coast and southern slope sub-regions. The northern coast is presumably highly influenced by sub-grid-scale phenomena that are not fully reproduced by the model, and which can potentially explain the poor model performance there; it is unclear at the moment why the model fails to capture MLD variability in the southern slope.

Interannual variability of the freshwater cycle in the region cannot be studied from the model results given that glacial inputs are based on estimated climatological values. However, because the model reasonably represents sea ice and is thought to have realistic values for meteoric sources, it is possible to do an assessment of the climatological importance of the different freshwater sources in the region in different seasons. Overall, the model is able to reproduce the basic patterns encountered in the observations, such as an onshore-offshore gradient in meteoric freshwater and more sea-ice melt in the coastal and southern region (compared to the northern part of the domain) in late summer. The regions of high sea-ice

melt in late summer are also regions of high sea-ice formation during the winter, and annual sea-ice melt values indicate net sea ice formation near the coast and in Marguerite Bay, with highest overall net sea-ice melt happening in the northern shelf of the domain.

Some of the changes to the model that could potentially improve the results further rely on phenomena for which there is very little data, such as circulation in the coastal ocean and Marguerite Bay, interannual variability of glacial freshwater discharges and sea-ice volume (thickness). Although the largest sea-ice thicknesses simulated by the model are of the order of one meter, which is in accordance with the scarce observations, data describing spatial and temporal changes in sea-ice volume are not available. More measurements on these properties would help quantify the freshwater cycle and its influence on surface water stratification. Since most data in the Southern Ocean are collected in areas of open ocean and during the summer, it is possible that there are biases in the initial conditions of ocean temperature and salinity used for the model.

Despite the biases in the model results, this study highlights the influence of sea-ice dynamics in the surface ocean mixing and freshwater fluxes, and the importance of proper choice of parameters when simulating sea ice. Although the model results suggest that using drag coefficients on the higher end of observed values leads to better results in this region of the WAP, it is important to consider that reanalysis products underestimate wind speed and therefore might be inducing the choice of higher drag coefficients to compensate for the model bias. The study also stresses the potential of Langmuir circulation in deepening the MLD in the Southern Ocean, and agrees with previous studies that the lack of properly parameterizing this phenomenon could be partially responsible for the shallow MLD seen in model results.

**Acknowledgements**

The authors thank the many scientists, students, technicians, and ship captains, officers and crew involved in the collection of the Palmer LTER historical time-series data. C. Schultz and S. Doney acknowledge support by the US National Science Foundation (grant PLR-1440435 to the Palmer Long Term Ecological Research program) and support from the University of Virginia. W. G. Zhang acknowledge support by the US National Science Foundation (grant OPP-1643901). The MITgcm model is an open source model (mitgcm.org). The version used in this study, with added parameterizations and specific configurations, are on C. Schultz's github (https://github.com/crisoceano/WAP_MITgcm). A copy of the files with specific configurations for this study, the forcing files needed for the simulations, and a copy of the files used for the KPP package are in three separate records on zenodo.org, under DOIs 10.5281/zenodo.3627365, 10.5281/zenodo.3627564, and 10.5281/zenodo.3627742.

## References


Andreas, E.L., Tucker, W.B. III & Ackley, S.F. (1984), Atmospheric boundary-layer modification, drag coefficient, and surface heat flux in the Antarctic marginal ice zone. *Journal of Geophysical Research*, 89 (C1): 649-661. doi:10.1029/JC089iC01p00649

Andreas, E.L., Horst, T.W., Grachev, A.A., Persson, P.O., Fairall, C.W., Guet, P.S. & Jordan, R.E. (2010), Parametrizing turbulent exchange over summer sea ice and the marginal ice zone. *Quarterly Journal of the Royal Meteorological Society*,136, 927-943. doi:10.1002/qj.618

Annett, A.L., Fitzsimmons, J.N., Séguret, M.J.M., Lagerström, M., Meredith, M.P., Schofield, O. & Sherrell, R.M. (2017), Controls on dissolved and particulate iron distributions in surface waters of the Western Antarctic Peninsula shelf. *Marine Chemistry*, 196, 81-97. doi:10.1016/j.marchem.2017.06.004.

Belcher, S.E., Grant, A.L.M., Hanley, K.E., Fox-Kemper, B., Van Roekel, L.,Sullivan, P.P., Large, W.G., Brown, A., Hines, A., Calvert, D., Rutgersson, A., Pettersson, H., Bidlot, J., Janssen, P.A.E.M. & Polton, J.A. (2012), A global perspective on Langmuir turbulence in the ocean surface boundary layer. *Geophysical Research Letters*, 39, L18605, 2012. doi:10.1029/2012GL052932

Birnbaum, G. & Lüpkes, C. (2002), A new parameterization of surface drag in the marginal ice zone. *Tellus A: Dynamic meteorology and Oceanography*, 54A: 107-123. doi:10.3402/tellusa.v54i1.12121

Boyer, T. P., Antonov, J. I., Baranova, O. K., Garcia, H. E., Johnson, D. R., Locarnini, R. A., Mishonov, A. V., O'Brien, T. D., Seidov, D., Smolyar, I. V. & Zweng, M. M. (2009), *World Ocean Database 2009, Chapter 1: Introduction*, in S. Levitus (ed.), NOAA Atlas NESDIS 66, World Ocean Database 2009, U.S. Gov. Printing Office, Wash. D.C., p. 216.

Bracegirdle, T.J., & Marshall, G.J. (2012), The reliability of Antarctic Tropospheric Pressure and Temperature in the latest Global Reanalyses. *Journal of Climate*, 25, 7138-7146. doi:10.1175/JCLI-D-11-00685.1

Castellani, G., Lüpkes, C., Hendricks, S. & Gerdes, R. (2014), Variability of sea-ice topography and its impact on the atmospheric surface drag. *Journal of Geophysical Research Oceans*, 119, 6743-6762. doi:10.1002/2013JC009712

Comiso, J. C. (2017). Bootstrap Sea Ice Concentrations from Nimbus-7 SMMR and DMSP SSM/I-SSMIS, Version 3. Boulder, Colorado USA. NASA National Snow and Ice Data Center Distributed Active Archive Center. doi: 10.5067/7Q8HCCWS4I0R

792 Cook, A.J., Fox, A.J., Vaughan, D.G. & Ferrigno, J.G. (2005), Retreating glacier fronts on the
793 Antarctic Peninsula over the past half-century. *Science*, 308, 541-544.
794 doi:10.1126/science.1104235
795
796 D'Asaro, E.A. (2014), Turbulence in the upper-ocean mixed layer, *Annual Reviews in Marine*
797 *Sciences*, 6, 101-115. doi:10.1146/annurev-marine-010213-135138
798
799 Dee, D. P., Uppala, S. M., Simmons, A. J., Berrisford, P., Poli, P., Kobayashi, S., Andrae, U.,
800 Balmaseda, M. A., Balsamo, G., Bauer, P., Bechtold, P., Beljaars, A. C. M., van de Berg, L., Bidlot,
801 J., Bormann, N., Delsol, C., Dragani, R., Fuentes, M., Geer, A. J., Haimberger, L., Healy, S. B.,
802 Hersbach, H., Holm, E. V., Isaksen, L., Kallberg, P., Kohler, M., Matricardi, M., McNally, A. P.,
803 Monge-Sanz, B. M., Morcrette, J.-J., Park, B.-K., Peubey, C., de Rosnay, P., Tavolato, C., Thepaut,
804 J.-N. & Vitart, F. (2011), The ERA-Interim reanalysis: configuration and performance of the data
805 assimilation system, *Quarterly Journal of the Royal Meteorological Society*, 137(656): 553–597.
806 doi:10.1002/qj.828
807
808 Doble, M. J., M. D. Coon & P. Wadhams (2003), Pancake ice formation in the Weddell Sea.
809 *Journal of Geophysical Research: Oceans*, 108(C7). doi:10.1029/2002JC001373
810
811 Ducklow, H.W., Fraser, W.R., Meredith, M.P., Stammerjohn, S.E., Doney, S.C, Martinson, D.G.,
812 Sailley, S.F., Schofield, O.M., Steinberg, S.K., Venables, H.J. & Amsler, C.D. (2013), West
813 Antarctic Peninsula: An ice-dependent coastal marine ecosystem in transition. *Oceanography*,
814 26(3), 190-203.
815
816 Fretwell, P., Pritchard, H.D., Vaughan, D.G., Bamber, J.L., Barrand, N.E., Bell, R., Bianchi, C.,
817 Bingham, R.G., Blankenship, D.D., Casassa, G., Catania,G., Callens, D., Conway, H., Cook, A.J.,
818 Corr, H.F.J., Damaske, D., Damm, V., Ferraccioli, F., Forsberg, R., Fujita, S., Gim, Y., Gogineni, P.,
819 Griggs, J.A., Hindmarsh, R.C.A., Holmlund, P., Holt, J.W., Jacobel, R.W., Jenkins, A.,Jokat, W.,
820 Jordan, T., King, E.C., Kohler, J., Krabill, W., Riger-Kusk, M., Langley, K.A., Leitchenkov, G.,
821 Leuschen, C., Luyendyk, B.P., Matsuoka, K., Mouginot, J., Nitsche, F.O., Nogi, Y., Nost, O.A.,
822 Popov, S.V., Rignot, E., Rippin, D.M., Rivera, A., Roberts, J., Ross, N., Siegert, M.J., Smith, A.M.,
823 Steinhage, D., Studinger, M., Sun, B., Tinto, B.K., Welch, B.C., Wilson, D., Young, D.A., Xiangbin,
824 C. & Zirizzotti, A. (2013), Bedmap2: improved ice bed, surface and thickness datasets for
825 Antarctica Cryosphere 7, 375–393. doi:10.5194/tc-7-375-2013
826
827 Grant, A. L. M. & S. E. Belcher (2009), Characteristics of Langmuir turbulence in the ocean mixed
828 layer. *Journal of Physical Oceanography*, 39, 1871–1887. doi:10.1175/2009JPO4119.1
829
830 Hauck, J., Völker, C., Wolf-Gladrow, D.A., Laufkötter, C., Vogt, M., Aumont, O., Bopp, L.,
831 Buitenhuis, E.T., Doney, S.C., Dunne, J., Gruber, N., Hashioka, T., John, J., Le Quéré, C., Lima,
832 I.D., Nakano, H., Séréfian & R., Totterdell, I. (2015), On the Southern Ocean $CO_2$ uptake and the
833 role of the biological carbon pump in the 21st century. *Global Biogeochemical Cycles*, 29, 1451-
834 1470. doi:10.1002/2015GB005140
835

836 Holland, P.R., Bruneau, N., Enright, C., Losch, M., Kurtz, N.T. & Kwok, R. (2014), Modeled Trends
837 in Antarctic Sea Ice thickness. *Journal of Climate*, 27, 3784-3801. doi:10.1175/JCLI-D-13-00301.1
838
839 Kim, H., Doney, S.C., Iannuzzi, R.A., Meredith, M.P., Martinson, D.G. & Ducklow, H.W. (2016),
840 Climate forcing for dynamics of dissolved inorganic nutrients at Palmer Station, Antarctica: An
841 interdecadal (1993–2013) analysis. *Journal of Geophysical Research: Biogeosciences*, *121* (9),
842 2369--2389. doi:10.1002/2015JG003311
843
844 Klinck, J.M., Hofmann, E.E., Beardsley, R.C., Salihoglu, B. & Howard, S. (2004), Watermass
845 properties and circulation on the west Antarctic Peninsula continental shelf in austral fall and
846 winter 2001. *Deep Sea Research Part II: Topical Studies in Oceanography*, V 51, issues 17-19,
847 1925-1946. doi:10.1016/j.dsr2.2004.08.001
848
849 Kohout, A. L., Williams, M. J. M., Dean, S. M., & Meylan, M. H. (2014), Storm-induced sea-ice
850 breakup and the implications for ice extent. *Nature*, 509, 604. doi:10.1038/nature13262
851
852 Large, W.G., McWilliams, J.C. & Doney, S.C. (1994), Oceanic vertical mixing: A review and a
853 model with a nonlocal boundary layer parameterization. *Reviews of Geophysics*, 32, 363-403.
854 doi: 10.1029/94RG01872
855
856 Legge, O.J., Bakker, D.C.E., Meredith, M.P., Venables, H.J., Brown, P.J., Jones, E.M. & Johnson,
857 M.T. (2017), The seasonal cycle of carbonate system processes in Ryder Bay, West Antarctic
858 Peninsula. *Deep Sea Research Part II: Topical Studies in Oceanography*, v. 139, 167-180. doi:
859 10.1016/j.dsr2.2016.11.006
860
861 Li, S., Li, M., Gerbi, G. P. & Song, J. (2013), Roles of breaking waves and Langmuir circulation in
862 the surface boundary layer of a coastal ocean. *Journal of Geophysical Research Oceans*, 118
863 (10): 5173-5187. doi: 10.1002/jgrc.20387
864
865 Li, Q., Fox-Kemper, B., Breivik, O & Webb, A. (2017), Statistical models of global Langmuir
866 mixing. *Ocean Modelling*, 113, 95-114. doi: 10.1016/j.ocemod.2017.03.016
867
868 Li, Q., & Fox-Kemper, B. (2017), Assessing the Effects of Langmuir Turbulence on the
869 Entrainment Buoyancy Flux in the Ocean Surface Boundary layer. *Journal of Physical*
870 *Oceanography*, v 47, 2863-2886. doi: 10.1175/JPO-D-17-0085.1
871
872 Losch, M. (2008), Modeling ice shelf cavities in a z coordinate ocean general circulation model.
873 *Journal of Geophysical Research*, 113(C8), C08043. doi: 10.1029/2007JC004368
874
875 Losch, M., Menemenlis, D., Campin, J.M., Heimbach, P. & Hill, C. (2010), On the formulation of
876 sea-ice models. Part 1: Effects of different solver implementations and parameterizations.
877 *Ocean Modelling*, 33, 129-144. doi: 10.1016/j.ocemod.2009.12.008
878

879 Marshall, J., Adcroft, A., Hill, C., Perelman, L. & Heisey, C. (1997), A finite-volume,
880 incompressible Navier-Stokes model for studies of the ocean on parallel computers. *Journal of*
881 *Geophysical Research*, 102, 5753-5766. doi: 10.1029/96JC02775
882
883 Marshall, J., Hill, C., Perelman, L. & Adcroft, A. (1997), Hydrostatic, quasi-hydrostatic, and
884 nonhydrostatic ocean modeling. *Journal of Geophysical Research*, 102(C3):5733-5752. doi:
885 10.1029/96JC02776
886
887 Martinson, D.G., Stammerjohn, S.E., Ianuzzi, R.A., Smith, R.C. & Vernet, M. (2008), Western
888 Antarctic Peninsula physical oceanography and spatio-temporal variability. *Deep-Sea Research*
889 *II*, 55, 1964-1987. doi: 10.1016/j.dsr2.2008.04.038
890
891 McWilliams, J.C. & Sulivan, P.P. (2000), Vertical mixing by Langmuir circulations. *Spill Science &*
892 *Technology Bulletin*, v 6, issues 3-4, 225-237. Doi: 10.1016/S1353-2561(01)00041-X
893
894 McWilliams, J.C., Huncke, E., Liang, J. & Sullivan, P.P. (2014), Langmuir turbulence in swell.
895 *Journal of Physical Oceanography*, 44, 870-890. doi: 10.1175/JPO-D-13-0122.1
896
897 Meredith, M.P. & King, J.C. (2005), Rapid climate change in the ocean west of the Antarctic
898 Peninsula during the second half of the 20$^{th}$ century. *Geophysical Research Letters*, 32, 1-5. doi:
899 10.1029/2005GL024042
900
901 Meredith, M.P., Brandon, M.A., Wallace, M.I., Clarke, A., Leng, M.J., Renfrew, I.A., van Lipzig,
902 N.P.M. & King, J.C. (2008), Variability in the freshwater balance of northern Marguerite Bay,
903 Antarctic Peninsula: results from $\Delta^{18}$O, *Deep Sea Research Part II: Topical Studies in*
904 *Oceanography*, 55, 309–322. doi: 10.1016/j.dsr2.2007.11.005
905
906 Meredith, M.P., Venables, H.J., Clarke, A., Ducklow, H.W., Erickson, M., Leng, M.J., Lenaerts,
907 J.T.M. & Van den Broeke, M.R. (2013), The Freshwater System West of the Antarctic Peninsula:
908 Spatial and Temporal Changes. *Journal of Climate*, 26, 1669-1684. doi: 10.1175/JCLI-D-12-
909 00246.1
910
911 Meredith, M.P., Stammerjohn, S.E., Venables, H.J., Ducklow, H.W., Martinson, D.G., Ianuzzi,
912 R.A., Leng, M.J., van Wessem, J.M., Reijmer, C.H. & Barrand, N.E. (2017), Changing distributions
913 of sea ice melt and meteoric water west of the Antarctic Peninsula. *Deep Sea Research Part II:*
914 *Topical Studies in Oceanography*. V. 129, 40-57. doi: 10.1016/j.dsr2.2016.04.019
915
916 Miller, P.A., Laxon, S.W., Feltham, D.L. & Cresswell, D.J. (2006), Optimization of sea ice model;
917 using basinwide observations of Arctic sea ice thickness, extent and velocity. *Journal of Climate*,
918 19, 1089-1108. doi: 10.1175/JCLI3648.1
919
920 Mitchell, B.G. & Holm-Hansen, O. (1991), Observations of modeling of the Antarctic
921 phytoplankton crop in relation to mixing depth. *Deep Sea Research Part A. Oceanographic*
922 *Research Papers*, v 38, issues 8-9, 981-1007.

Moffat, C., Beardsley, R.C., Owens, B. & van Lipzig, N. (2008), A first description of the Antarctic Peninsula Coastal Current. *Deep-Sea Research Part II, Topical Studies in Oceanography*, 55, 277-293. doi: 10.1016/j.dsr2.2007.10.003

Moffat, C. & Meredith, M. (2018), Shelf–ocean exchange and hydrography west of the Antarctic Peninsula: a review. *Philosophical Transactions of the Royal Society A*, 376: 20170164. doi: 10.1098/rsta.2017.0164

Noh, Y. & Lee, W.S. (2008), Prediction of the mixed and mixing layer depths from an OGCM. *Journal of Oceanography*, 64, 217-225. doi:10.1007/s10872-008-0017-1.

Phillips, O.M. (1985), Spectral and statistical properties of the equilibrium range in wind-generated gravity waves. *Journal of Fluid Mechanics*, 156, 505-531. doi:10.1017/S0022112085002221

Regan, H.C., Holland, P.R., Meredith, M.P. & Pike, J. (2018), Sources, variability and fate of freshwater in the Bellingshausen Sea, Antarctica. *Deep-Sea Research Part I: Oceanographic Research Papers,* 133, 59-71. doi: 10.1016/j.dsr.2018.01.005

Schiller, A. & Ridgway., K.R. (2013), Seasonal mixed-layer dynamics in an eddy-resolving ocean circulation model. *Journal of Geophysical Research Oceans*, 118, 3387-3405. Doi:10.1002/jgrc.20250

Smith, M., Stammerjohn, S., Persson, O., Rainville, L., Liu, G. & Perrie, W. (2018), Episodic reversal of autumn ice advance caused by release of ocean heat in the Beaufort Sea. *Journal of Geophysical Research: Oceans*, 123, 3164–3185. doi:10.1002/2018JC013764

Stammerjohn, S.E., Martinson, D.G., Smith, R.C. & Ianuzzi, R.A. (2008), Sea ice in the western Antarctic Peninsula region: Spatio-temporal variability from ecological and climate change perspectives. *Deep-Sea Research Part II*, 55, 2041-2058. doi: 10.1016/j.dsr2.2008.04.026

Stammerjohn, S., Massom, R. A., Rind, D., & Martinson, D. (2012), Regions of rapid sea ice change: An inter-hemispheric seasonal comparison. *Geophysical Research Letters*, *39* (L06501). doi: 10.1029/2012GL050874

Talley, L.D., Pickard, G.L., Emery, W.J. & Swift, J.H. (2011), Descriptive Physical Oceanoraphy: An Introduction (sixth edition), Elsevier, Boston, 560 pp.

Taylor, M.H., Losch, M. & Bracher, A. (2013), On the drivers of phytoplankton blooms in the Antarctic marginal ice zone: a modeling approach. *Journal of Geophysical Research: Oceans*, 118, 63-75. doi: 10.1029/2012JC008418

Tsamados, M., Feltham, D.L., Schroeder, D. & Flocco, D. (2014), Impact of variable atmospheric and oceanic form drag on simulations of Arctic sea ice. *Journal of Physical Oceanography*, 44(5), 1329-1353. doi: 10.1175/JPO-D-13-0215.1

Turner, J., Lu, H., White, I., King, J.C., Phillips, T., Hosking, J.S., Bracegirdle, T.J., Marshall, G.J., Mulvaney, R. & Deb, P. (2016), Absence of 21$^{st}$ century warming on Antarctic Peninsula consistent with natural variability. *Nature*, 535, 411–415. doi: 10.1038/nature18645

Van Wessem, J.M., Meredith, M.P., Reijmer, C.H., van den Broeke, M.R. & Cook, A.J. (2016), Characteristics of the modelled meteoric freshwater budget of the western Antarctic Peninsula, *Deep Sea Research Part II: Topical Studies in Oceanography*, 139, 31-39. doi:10.1016/j.dsr2.2016.11.001

Vaughan, D.G., Marshall, G.J., Connolley, W.M., Parkingson, C., Mulvaney, R., Hodgson, D.A., King, J.C., Pudsey, C.J. & Turner, J. (2003), Recent Rapid Regional Climate Warming on the Antarctic Peninsula. *Climatic Change*, 60, 243-274, 2003. doi: 10.1023/A:1026021217991

Vernet, M., Martinson, D., Ianuzzi, R., Stammerjohn, S., Kozlowski, W., Sines, K., Smith, R. & Garibotti, I. (2008), Primary production within the sea-ice zone west of the Antarctic Peninsula: I – Sea ice, summer mixed layer, and irradiance. *Deep-Sea Research Part II*, 55, 2068-2085. doi: 10.1016/j.dsr2.2008.05.021

Wamser, C. & Martinson, D.G. (1993), Drag Coefficients for Winter Antarctic Pack Ice. Journal of Geophysical Research: Oceans, v. 98 (C7), 12,431-12,437. doi:10.1029/93JC00655

Webb, A., & Fox-Kemper, B. (2015), Impacts of wave spreading and multidirectional waves on estimating stokes drift. *Ocean Modelling*, 96, 49-64. doi: 10.1016/j.ocemod.2014.12.007

Journal of Geophysical Research: Oceans

# Modeling of the Influence of Sea Ice Cycle and Langmuir Circulation on the Upper Ocean Mixed Layer Depth and Freshwater Distribution at the West Antarctic Peninsula

**C. Schultz[1], S. C. Doney[1], W. G. Zhang[2], H. Regan[3], P. Holland[4], M. Meredith[4], S. Stammerjohn[5]**

[1] University of Virginia, Department of Environmental Sciences, Charlottesville, VA, USA
[2] Woods Hole Oceanographic Institution, Woods Hole, MA, USA
[3] Univ. Brest, CNRS, IRD, Ifremer, Laboratoire D'Océanographie Physique et Spatiale, IUEM, Brest, France
[4] British Antarctic Survey, Natural Environment Research Council, Cambridge, UK
[5] Institute of Arctic and Alpine Research, University of Colorado, Boulder, CO, USA

Corresponding author: Cristina Schultz (cs3xm@virginia.edu)

**Contents of this file**

Figures S1 to S5
Tables S1 to S4

## Introduction

The data used to make the figures and tables in this document is the same as described in the methods section in the article.

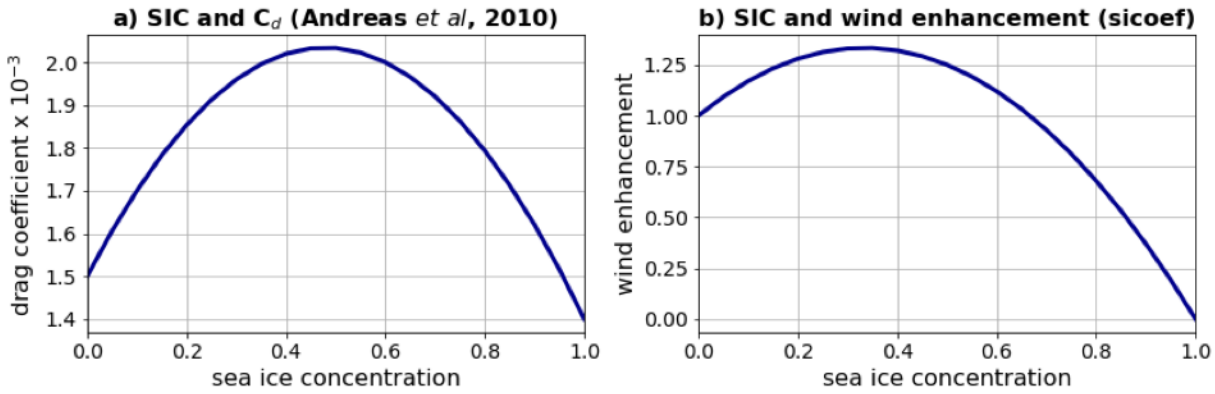


Figure S1: a) Relationship between wind-sea-ice drag coefficient (Cd) and sea ice concentration from Andreas et al (2010); b) Relationship between the wind enhancement factor (sicoef) and sea ice concentration used in this study.

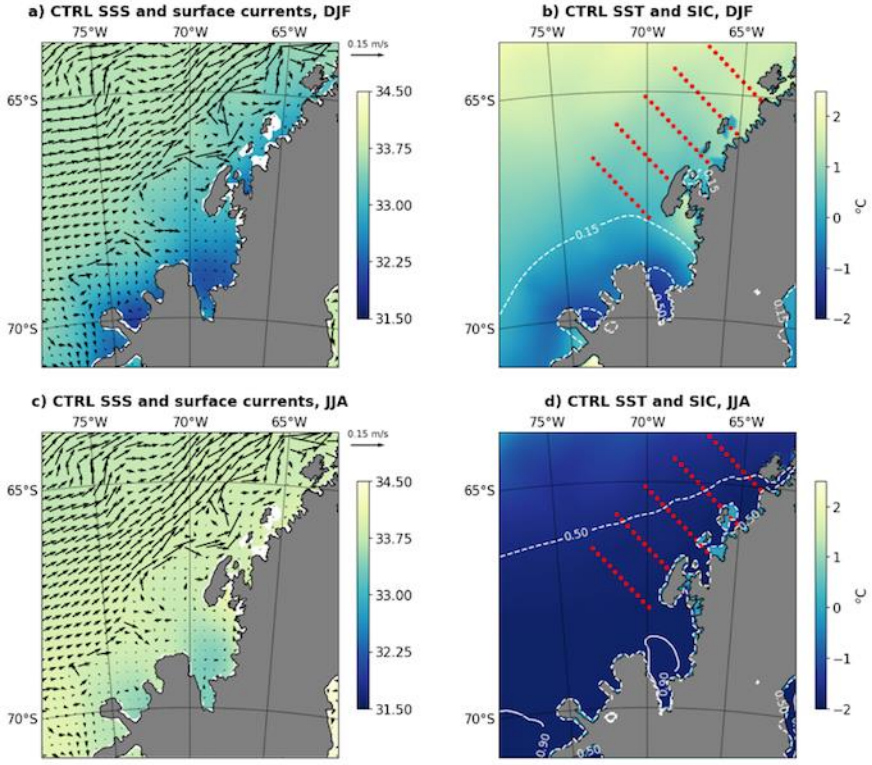


Figure S2: Simulated climatology (from CTRL integration) of A) sea surface salinity (color), surface currents (arrows), B) Sea surface temperature (color) and sea ice concentration (white dashed line) during the summer (December-February); climatology of C) sea surface salinity (color), surface currents (arrows), D) sea surface temperature and sea ice concentration during winter (June-August). The red dots on panels B and D represent the location of the Palmer-LTER cruise stations.

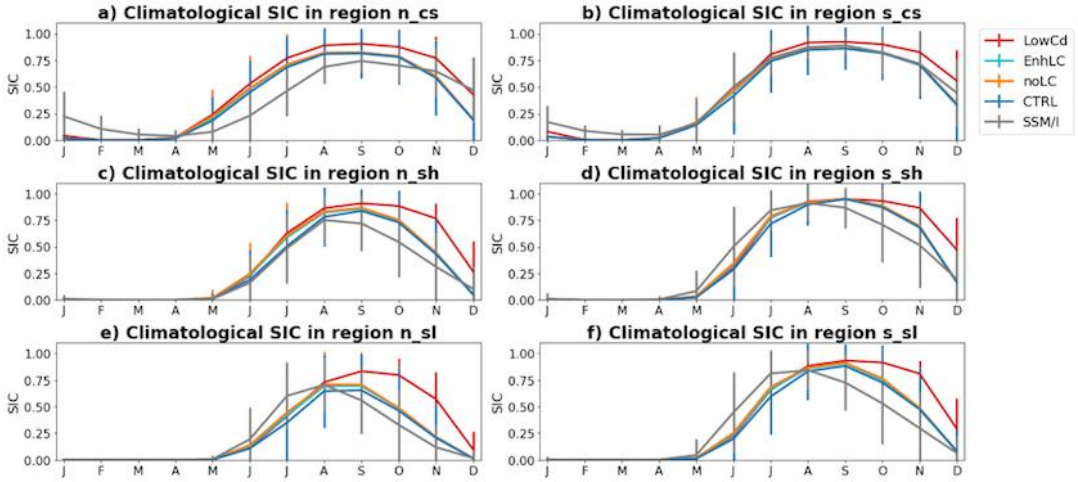


Figure S3: Monthly climatology of sea ice concentration from the satellite observations (SSM/I; grey) and from the model simulations (other color). Vertical bars indicate standard deviation between the monthly means of each year.

Although onset times of sea-ice advance and retreat offer valuable information on the interannual variability of sea-ice dynamics in the region, climatological monthly means of SIC (Figure S3) provides information on how each simulation compares to observations throughout the year. In the northern coastal region, the model showed lower variability compared to the satellite data, evidenced by the lower standard deviation; and had a faster increase and decrease in SIC during advance and retreat of sea ice, leading to higher SIC in the winter and lower in the summer when compared to observations. In the southern coastal region, the model simulation shows a somewhat faster decrease of sea ice during summer months, with lower SIC during January and February, but the advance of sea ice is well captured. In the shelf and slope region, modeled sea-ice retreat happened later than the observed, and although sea-ice advance had a similar start date the observations, the observations had a faster increase of SIC.

Comparing the SIC climatologies from the CTRL and LowCd results, it is seen that lower drag coefficient leads to later sea-ice retreat in all sub-regions. High SIC persists in LowCd well into October (November) in the slope (shelf), with SIC higher than 0.75 while observations and CTRL show concentrations during that period below 0.5. The differences in sea-ice advance are less pronounced. Simulations noLC and EnhLC have similar SIC to LowCd during the season of sea ice advance, suggesting that wind action is not the cause of the SIC discrepancy. Different treatments for LC did not affect the retreat of sea ice, confirming the previous assessment that wind action is more important for retreat of sea ice than for its advance.

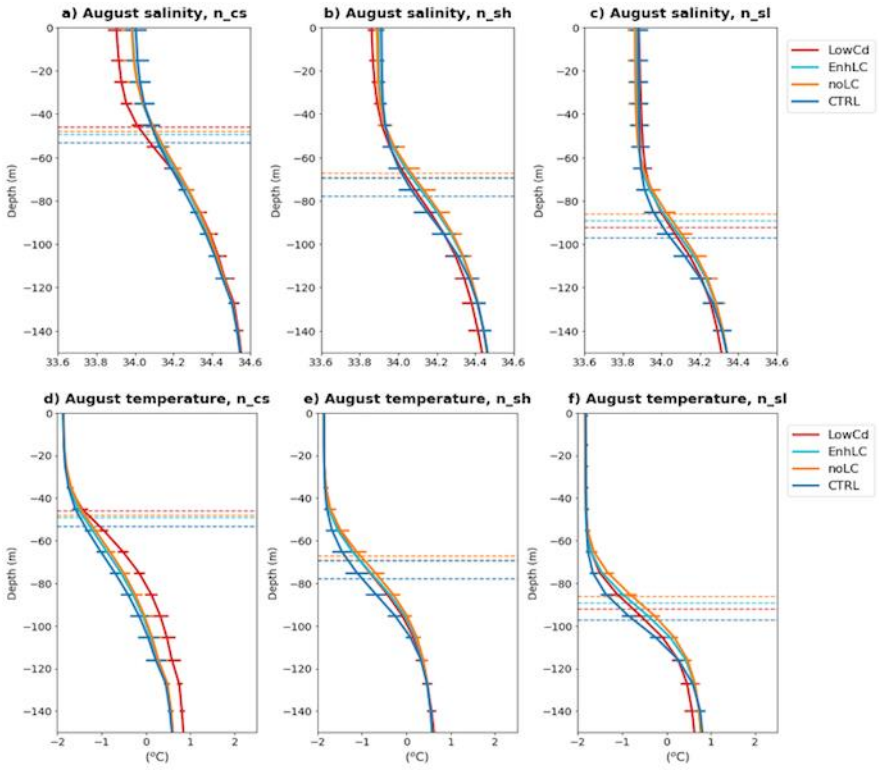


Figure S4: Simulated August salinity climatology for (a) northern coast, (b) northern shelf and (c) northern slope regions; and simulated August climatology of temperature for (d) northern coast, (e) northern shelf and (f) northern slope regions. Horizontal solid lines represent standard deviation, and horizontal dashed lines indicate climatological MLD for the period considered.

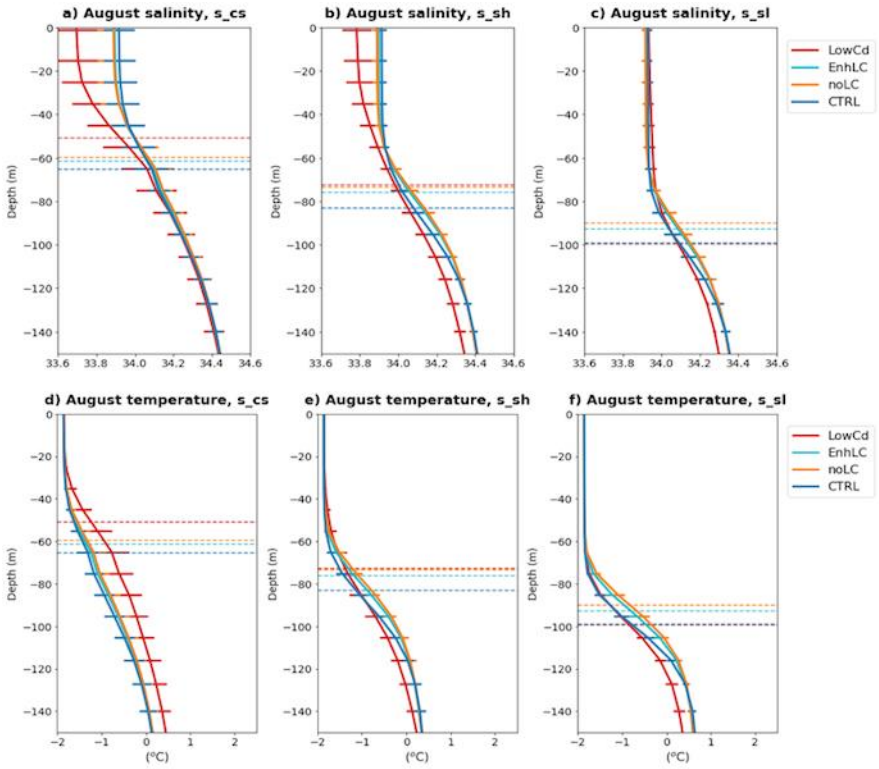


Figure S5: Simulated August climatology of salinity for (a) southern coast, (b) southern shelf and (c) southern slope regions; and simulated August climatology of temperature for (d) southern coast, (e) southern shelf and (f) southern slope regions. Horizontal solid lines represent standard deviation, and horizontal dashed lines indicate climatological MLD for the period considered.

| **Experiment Name** | **Cd** | **LC Parameterization** |
|---|---|---|
| CTRL<br>(control simulation) | $2*10^{-3}$ | Li and Fox-Kemper (2017) |
| LowCd<br>(simulation with lower Cd value) | $5*10^{-4}$ | Li and Fox-Kemper (2017) |
| noLC<br>(simulation with no LC parameterization) | $2*10^{-3}$ | None |
| EnhLC<br>(Enhanced LC simulation) | $2*10^{-3}$ | Li et al (2017) |

Table S1: Values of air-sea ice drag coefficient (*Cd*) and choices of Langmuir circulation parameterization in each simulation.

| | s_cs | s_sh | s_sl | n_cs | n_sh | n_sl |
|---|---|---|---|---|---|---|
| CTRL | 0.87 | 0.82 | 0.92 | 0.62 | 0.70 | 0.86 |
| noLC | 0.75 | 0.88 | 0.86 | 0.52 | 0.72 | 0.81 |
| LowCd | 0.44 | 0.80 | 0.92 | 0.44 | 0.66 | 0.81 |
| EnhLC | 0.75 | 0.89 | 0.85 | 0.64 | 0.72 | 0.80 |

Table S2: Correlation between modeled and observed times of sea ice advance. All correlations are significant at 95% confidence level. Location of stations for each sub-region are shown in Figure 1B, and description of simulations are shown in Table S1.

| | **s_cs** | **s_sh** | **s_sl** | **n_cs** | **n_sh** | **n_sl** |
|---|---|---|---|---|---|---|
| CTRL | 0.87 | 0.86 | 0.81 | 0.89 | 0.85 | 0.82 |
| noLC | 0.85 | 0.83 | 0.75 | 0.91 | 0.86 | 0.79 |
| LowCd | 0.51 | 0.27 | 0.61 | 0.67 | 0.44 | 0.58 |
| EnhLC | 0.85 | 0.84 | 0.77 | 0.91 | 0.86 | 0.80 |

Table S3: Correlation between modeled and observed times of sea ice retreat. All correlations, with the exception of LowCd at s_sh, are significant at 95% confidence level. Location of stations for each sub-region are shown in Figure 1B, and description of simulations are shown in Table S1.

| | **n_cs** | **n_sh** | **n_sl** | **s_cs** | **s_sh** | **s_sl** |
|---|---|---|---|---|---|---|
| CTRL | 0.308 | 0.703 | 0.596 | 0.575 | 0.932 | 0.110 |
| noLC | 0.322 | 0.580 | 0.534 | 0.574 | 0.843 | 0.125 |
| LowCd | 0.229 | 0.417 | 0.486 | 0.437 | 0.698 | 0.170 |
| EnhLC | 0.301 | 0.604 | 0.554 | 0.563 | 0.859 | 0.142 |

TableS 4: Correlation coefficient between simulated average MLD for January-February each year and Palmer-LTER average MLD for each cruise in each sub-region. Numbers in bold are significant at 95% confidence level. Location of stations for each sub-region are shown in Figure 1B, and description of simulations are shown in Table S1.